PNAS RESEARCH ARTICLE | IMMUNOLOGY AND INFLAMMATION OPEN ACCESS

Elevated Myl9 reflects the Myl9-containing microthrombi in SARS-CoV-2–induced lung exudative vasculitis and predicts COVID-19 severity

Chiaki Iwamura[a], Kiyoshi Hirahara[a,1], Masahiro Kiuchi[a], Sanae Ikehara[b], Kazuhiko Azuma[b], Tadanaga Shimada[c], Sachiko Kuriyama[a], Syota Ohki[b], Emiri Yamamoto[b], Yosuke Inaba[d], Yuki Shiko[d], Ami Aoki[a], Kota Kokubo[a], Rui Hirasawa[a], Takahisa Hishiya[a], Kaori Tsuji[a], Tetsutaro Nagaoka[e], Satoru Ishikawa[f], Akira Kojima[f], Haruki Mito[g], Ryota Hase[g], Yasunori Kasahara[h], Naohide Kuriyama[i], Tetsuya Tsukamoto[j], Sukeyuki Nakamura[k], Takashi Urushibara[l], Satoru Kaneda[m], Seiichiro Sakao[n], Minoru Tobiume[o], Yoshio Suzuki[o], Mitsuhiro Tsujiwaki[p], Terufumi Kubo[p], Tadashi Hasegawa[p], Hiroshi Nakase[q], Osamu Nishida[j], Kazuhisa Takahashi[e], Komei Baba[r], Yoko Iizumi[s], Toshiya Okazaki[s], Motoko Y. Kimura[t], Ichiro Yoshino[u], Hidetoshi Igari[v,w], Hiroshi Nakajima[w,x], Takuji Suzuki[n], Hideki Hanaoka[d], Taka-aki Nakada[c], Yuzuru Ikehara[b,y], Koutaro Yokote[z], and Toshinori Nakayama[a,aa,1]

Edited by Max Cooper, Emory University, Atlanta, GA; received February 25, 2022; accepted June 22, 2022

The mortality of coronavirus disease 2019 (COVID-19) is strongly correlated with pulmonary vascular pathology accompanied by severe acute respiratory syndrome coronavirus 2 (SARS-CoV-2) infection–triggered immune dysregulation and aberrant activation of platelets. We combined histological analyses using field emission scanning electron microscopy with energy-dispersive X-ray spectroscopy analyses of the lungs from autopsy samples and single-cell RNA sequencing of peripheral blood mononuclear cells to investigate the pathogenesis of vasculitis and immunothrombosis in COVID-19. We found that SARS-CoV-2 accumulated in the pulmonary vessels, causing exudative vasculitis accompanied by the emergence of thrombospondin-1–expressing noncanonical monocytes and the formation of myosin light chain 9 (Myl9)–containing microthrombi in the lung of COVID-19 patients with fatal disease. The amount of plasma Myl9 in COVID-19 was correlated with the clinical severity, and measuring plasma Myl9 together with other markers allowed us to predict the severity of the disease more accurately. This study provides detailed insight into the pathogenesis of vasculitis and immunothrombosis, which may lead to optimal medical treatment for COVID-19.

COVID-19 | exudative vasculitis | nonconventional monocytes | microthrombi | plasma Myl9

Severe acute respiratory syndrome coronavirus 2 (SARS-CoV-2) is a highly transmissible and pathogenic coronavirus causing coronavirus disease 2019 (COVID-19) and affecting billions of people worldwide. COVID-19 patients showed a higher mortality rate during hospitalization than patients with influenza infection (1). The fatality rate due to COVID-19 was ∼1 to 2%, depending on the age of the patient, the presence or absence of underlying diseases, and the location of residence (2, 3). Although vaccination is effective in preventing the onset and severity of COVID-19, globally, weekly confirmed deaths due to COVID-19 continued to be ∼20,000 to 30,000 as of April 2022 (https://coronavirus.jhu.edu/map.html). Recent studies have shown that age, sex, and certain underlying diseases are risk factors for severe COVID-19 (3–6). Immunological studies also revealed that a deficiency of type I interferons (IFNs) due to neutralizing autoantibodies or genetic defects in type I IFN signaling is involved in the severity of COVID-19 (7–10). Clarifying the pathogenesis of COVID-19 and developing new therapeutic interventions are extremely important because of the high mortality rate of COVID-19 and the continual appearance of new virus variants that can evade the host immune response induced by vaccination (11).

Accumulating evidence indicates that ∼20% of deceased COVID-19 patients had autoantibodies that neutralize type 1 IFNs (9). At the same time, hyperinflammation caused by low IFN responses and excessive viral replication leads to severe COVID-19 (12, 13). Immune profiling in peripheral blood or bronchoalveolar lavage fluid has revealed that the most prominent changes in the immune system include excessive neutrophil activation, lymphopenia, dysregulated myeloid cells, and aberrant responses of the adaptive immune systems (14–18). Histological analyses of autopsy samples from patients who died with COVID-19 have revealed that the lungs display distinctive vascular features, consisting of endothelial injury associated with cellular infiltration and microthrombi (19). Regarding the vascular pathology, adult patients with critical COVID-19 can develop cutaneous vasculitis and systemic arterial and venous thromboemboli (20, 21). Notably, pulmonary thrombus was more frequent in fatal COVID-19

Significance

Elucidation of the pathology triggered by SARS-CoV-2 infection is essential to control the pandemic. We found that severe acute respiratory syndrome coronavirus 2 (SARS-CoV-2) accumulates in the pulmonary vessels, causing exudative vasculitis accompanied by the emergence of noncanonical monocytes that specifically produce a platelet activating factor, thrombospondin-1, and the formation of myosin light chain 9 (Myl9)–containing microthrombi in the lungs of coronavirus disease 2019 (COVID-19) patients with fatal disease. More interestingly, we demonstrate that SARS-CoV-2–induced platelet activation causes an increase in the plasma Myl9 level, which is closely correlated with clinical severity. The measurement of plasma Myl9 with other markers allowed us to diagnose the severity of the disease more accurately, which is crucial for providing appropriate medical care for COVID-19 patients.

This article is a PNAS Direct Submission.

[1]To whom correspondence may be addressed. Email: hiraharak@chiba-u.jp or tnakayama@faculty.chiba-u.jp.

This article contains supporting information online at http://www.pnas.org/lookup/suppl/doi:10.1073/pnas.2203437119/-/DCSupplemental.

Published July 27, 2022.

cases than in those who died of influenza (22). Indeed, an increased level of D-dimer, which reflects the activation of the coagulation system, is associated with a poor prognosis (23). However, the details concerning the cascade of pathological and immunological events and the critical factors involved in innate and adaptive immunity in immunothrombosis accompanied by vasculitis in critical COVID-19 remain unclear.

We found that SARS-CoV-2 infection caused exudative vasculitis as well as the accumulation of SARS-CoV-2 elements in the middle smooth muscle layer of the arteries in the lungs of fatal COVID-19 cases. Single-cell RNA-sequencing (scRNA-seq) analyses revealed increased numbers of myeloid cells with biased up-regulation of platelet-activating signature, especially thrombospondin-1 (THBS-1)–expressing noncanonical monocytes. Microthrombi accompanied by the deposition of myosin light chain 9 and 12 (Myl9/12) were detected in the arteries of the lungs of fatal COVID-19 cases. The concentration of plasma Myl9 was significantly increased in COVID-19 patients. More importantly, we have found that the plasma Myl9 level reflects the clinical condition of COVID-19 patients. Plasma Myl9 will be a biomarker to predict the severity of COVID-19 and a potential therapeutic target for preventing microthrombosis and intractable vasculitis in COVID-19.

Results

Introduction to the Patient Cohort. All of the patients enrolled in this study were diagnosed with or denied to have COVID-19 based on positive and negative RT-PCR findings, respectively, and stratified according to disease severity (24, 25) (*SI Appendix*, Table S1). To assess the impact of SARS-CoV-2 infection on both local inflammatory sites and the systemic immune system, we analyzed five autopsy samples, including three individuals who died with COVID-19, one that died with stomach cancer, and one that died with hereditary diffuse leukoencephalopathy (cohort 1) (Table 1 and *SI Appendix*, Fig. S1 *A*, *Upper*), and 177 whole-blood samples, including 123 from individuals with COVID-19 (cohort 2) (*SI Appendix*, Fig. S1 *A*, *Lower*). Of the 123 patients with COVID-19 in cohort 2, we collected blood samples once a week from moderate or severe patients and every 3 d from critical patients, with a total of 400 samples obtained.

Regarding patients' information, their medical conditions revealed that the patients enrolled in this study showed phenotypic characteristics of COVID-19 (Table 2). Of all patients enrolled in cohort 2, almost half of the patients ($n = 60$) showed moderate symptoms, while the other half ($n = 63$) showed more severe symptoms. The median age of the enrolled patients was 57 y. Female patients account for 33% of all patients, and the proportion of female patients was decreased in more severe groups. The numbers of patients with higher body mass index (BMI) values or complications, such as hypertension and diabetes, were increased in more severe groups. The lactate dehydrogenase (LDH), D-dimer, C-reactive protein (CRP), and ferritin levels, the neutrophil count, and the levels of plasma inflammatory cytokines, such as interleukin (IL)-6, IL-8, IP-10, and MCP-1, increased in correlation with the severity of COVID-19 (*SI Appendix*, Fig. S1*B*). These results indicate that our cohort 2 recapitulated the findings of previous reports (3–5, 26).

Aggregated SARS-CoV-2 Particles Disrupted the Tunica Media, Resulting in Exudative Changes in the Bronchovascular Space. We first assessed the lung autopsy material from three individuals with COVID-19 to investigate the pathological impact of SARS-CoV-2 infection in the lungs (cases #1 to #3) (Table 1). Notably, case #2 suffered from mucormycosis, which has been described in several other studies, especially in India (27–29). A representative figure from a computed tomography (CT) analysis of case #2 showed pneumonia characteristic of COVID-19

Table 1. Clinical characteristics of COVID-19 patients with autopsy

Variable	Case #1	Case #2*	Case #3
Age (y)	86	58	80
Sex	Male	Male	Male
Comorbidity	None	Diabetes Hypertension Idiopathic pulmonary fibrosis Dyslipidemia	Diabetes Hypertension Dyslipidemia Prostatic hyperplasia
Treatments			
Steroid	None	+	+
Antivirus		+	+
Antibiotics		+	+
Anticoagulant		—	+
Hospitalization (on admission-deceased)	3/7/21 to 3/7/21	11/28/20 to 12/30/20	3/11/20 to 03/28/20
PCR test result	Positive (3/7/20), negative (not tested)	Positive (11/27/20), negative (12/1/20)	Positive (3/12/20), negative (not tested)
MV (d)	0	30	15
ECMO (d)	0	21	0
Complication	None	Mucormycosis Pancreatitis Pulmonary and renal infarction Nonocclusive mesenteric ischemia Cerebral hemorrhage	Renal failure Anemia Liver dysfunction
Cause of death	Acute respiratory distress syndrome	Multiple organ failure	COVID-19 pneumonia

ECMO, Extracorporeal membrane oxygenation; MV, mechanical ventilation.
*The details about case #2 are described in a published case report (28).

Table 2. Characteristics of the enrolled COVID-19 patients

	Total n = 123	Moderate n = 60 (48.8%)	Severe n = 24 (19.5%)	Critical n = 27 (22.0%)	Fatal n = 12 (9.8%)
Demographics and sex					
Age, median (± SD)	57 (15.2)	48 (15.1)	61.5 (11.6)	58 (13.3)	68.5 (8.9)
20–29 y old	11 (8.9)	10 (16.7)	1 (4.2)	0 (0.0)	0 (0.0)
30–39 y old	12 (9.8)	10 (16.7)	0 (0.0)	2 (7.4)	0 (0.0)
40–49 y old	19 (15.4)	12 (20.0)	0 (0.0)	6 (22.2)	1 (8.3)
50–59 y old	33 (26.8)	15 (25.0)	10 (41.7)	6 (22.2)	2 (16.7)
60–69 y old	28 (22.8)	8 (13.3)	8 (33.3)	8 (29.6)	4 (33.3)
70–79 y old	16 (13.0)	4 (6.7)	4 (16.7)	3 (11.1)	5 (41.7)
80–89 y old	4 (3.3)	1 (1.7)	1(4.2)	2 (7.4)	0 (0.0)
Female	33 (26.8)	24 (40.0)	2 (8.3)	5 (18.5)	2 (16.7)
BMI					
<25	56 (45.5)	36 (60.0)	8 (33.3)	10 (37.0)	2 (16.7)
25 to <30	48 (39.0)	20 (33.3)	12 (50.0)	11(40.7)	5 (41.7)
30 to <40	10 (8.1)	3 (5.0)	2 (8.3)	2 (7.4)	3 (25.0)
≥40	4 (3.3)	0 (0.0)	0 (0.0)	3 (11.1)	1 (8.3)
Not recorded	5 (4.1)	1 (1.7)	2 (8.3)	1 (3.7)	1 (8.3)
BMI, Average (± SD)	25.6 (6.0)	23.8 (3.9)	25.7 (2.9)	28.2 (9.3)	28.9 (5.7)
Complications					
Hypertension	36 (29.3)	11 (18.3)	9 (37.5)	10 (37.0)	6 (50.0)
Diabetes	31 (25.2)	6 (10.0)	7 (29.2)	13 (48.1)	5 (41.7)
Dyslipidemia	26 (21.1)	8 (13.3)	10 (41.7)	6 (22.2)	2 (16.7)
Hyperuricemia	16 (13.0)	5 (8.3)	7 (29.2)	2 (7.4)	2 (16.7)
Respiratory diseases	12 (9.8)	2 (3.3)	1 (4.2)	8 (29.6)	1 (8.3)
Duration of hospital stay, d (IQR)	11 (9–22)	9 (8–10)	12 (11–18)	31 (17–48)	30 (17–41)
Medications					
Corticosteroid	69 (56.1)	9 (15.0)	22 (91.7)	26 (96.3)	12 (100.0)
Antiviral	74 (60.2)	15 (25.0)	24 (100.0)	24 (88.9)	11 (91.7)
Antibiotic	26 (21.1)	1 (1.7)	2 (8.3)	16 (59.3)	7 (58.3)
Anticoagulant	43 (35.0)	3 (5.0)	8 (33.3)	22 (81.5)	10 (83.3)
Tocilizumab	18 (14.6)	0 (0.0)	2 (8.3)	10 (37.0)	6 (50.0)
Treatments					
Mechanical ventilation	37 (30.1)	0 (0.0)	0 (0.0)	26 (96.3)	11 (91.7)
ECMO	15 (12.2)	0 (0.0)	0 (0.0)	7 (25.9)	8 (66.7)
CHDF	14 (11.42)	0 (0.0)	0 (0.0)	6 (22.2)	8 (66.7)
Apheresis	7 (5.7)	0 (0.0)	1 (4.2)	4 (14.8)	2 (16.7)
Nitric oxide	16 (13.0)	0 (0.0)	0 (0.0)	11 (40.7)	5 (41.7)
Prone position	10 (8.1)	0 (0.0)	0 (0.0)	6 (22.2)	4 (33.3)

Data are presented as No. (%) unless indicated otherwise. CHDF, continuous hemodiafiltration.

(*SI Appendix*, Fig. S1*C*). Histological analyses of lung samples from all patients revealed features characteristic of diffuse alveolar damage, with hypercellular thickening of the alveolar septa, fibrosis, hyaline membrane, and extensive cellular infiltration (*SI Appendix*, Fig. S1*D*). Using immunohistochemistry, distinct immunoreactivity for the spike protein of SARS-CoV-2 was detected in the vascular wall in samples from fatal COVID-19 cases (Fig. 1 *A Upper*, black arrowheads) but not in control samples (Fig. 1 *A*, *Lower*). On the ultrastructural level, aggregated SARS-CoV-2 particles were detected in the tunica media by field emission scanning electron microscopy (FE-SEM), by specific spike protein antibody and Cobalt labeled 3, 3′-diaminobenzidine (DAB) using energy-dispersive X-ray spectroscopy (EDX) (Fig. 1*B* and *SI Appendix*, Fig. S1*E*). Elastin van Gieson (EVG) staining of the lung samples revealed thickening and disruption of elastic fibers in the SARS-CoV-2–infected arteries (Fig. 1 *C*, *Upper*), while thin layers of elastic fibers were found in the arteries of control samples (Fig. 1 *C*, *Lower*). Consistent with disruption of the tunica media, the tunica adventitia and bronchovascular space showed characteristic histological features of exudative inflammation with tearing and thickening of the elastic fibers in the vessel wall accompanied by dilation of the adventitia (Fig. 1 *D*, *Left*, black arrowhead) and enlargement of the lymphatics (Fig. 1 *D*, *Left*, white arrowhead). A significant increase in the dimensions of the adventitia was detected in the lungs of fatal COVID-19 cases compared with the control lungs (Fig. 1 *D*, *Right*). In contrast, the typical features of exudative vasculitis were not observed in the kidneys of cases #1 and #2 (*SI Appendix*, Fig. S1*F*). These findings revealed that the arteries in the lungs of fatal COVID-19 cases showed exudative vasculitis together with the presence of SARS-CoV-2 elements in the arterial blood vessels.

Single-Cell Transcriptome Profiling Reveals Dysregulation of Myeloid Cells with Biased Up-Regulation of Platelet-Activating Signature in the Blood of Critical and Fatal COVID-19 Cases. To clarify the functional states of systemic immune cells in COVID-19, we next conducted transcriptome profiling by scRNA-seq for blood samples from 21 patients (10 moderate, 6 critical, and 5 fatal cases in our cohort 2) (*SI Appendix*, Fig. S1*A*). The blood samples used for scRNA-seq were collected on admission (n = 13) or within 10 d of admission (n = 8). A total of 57,049 single-cell

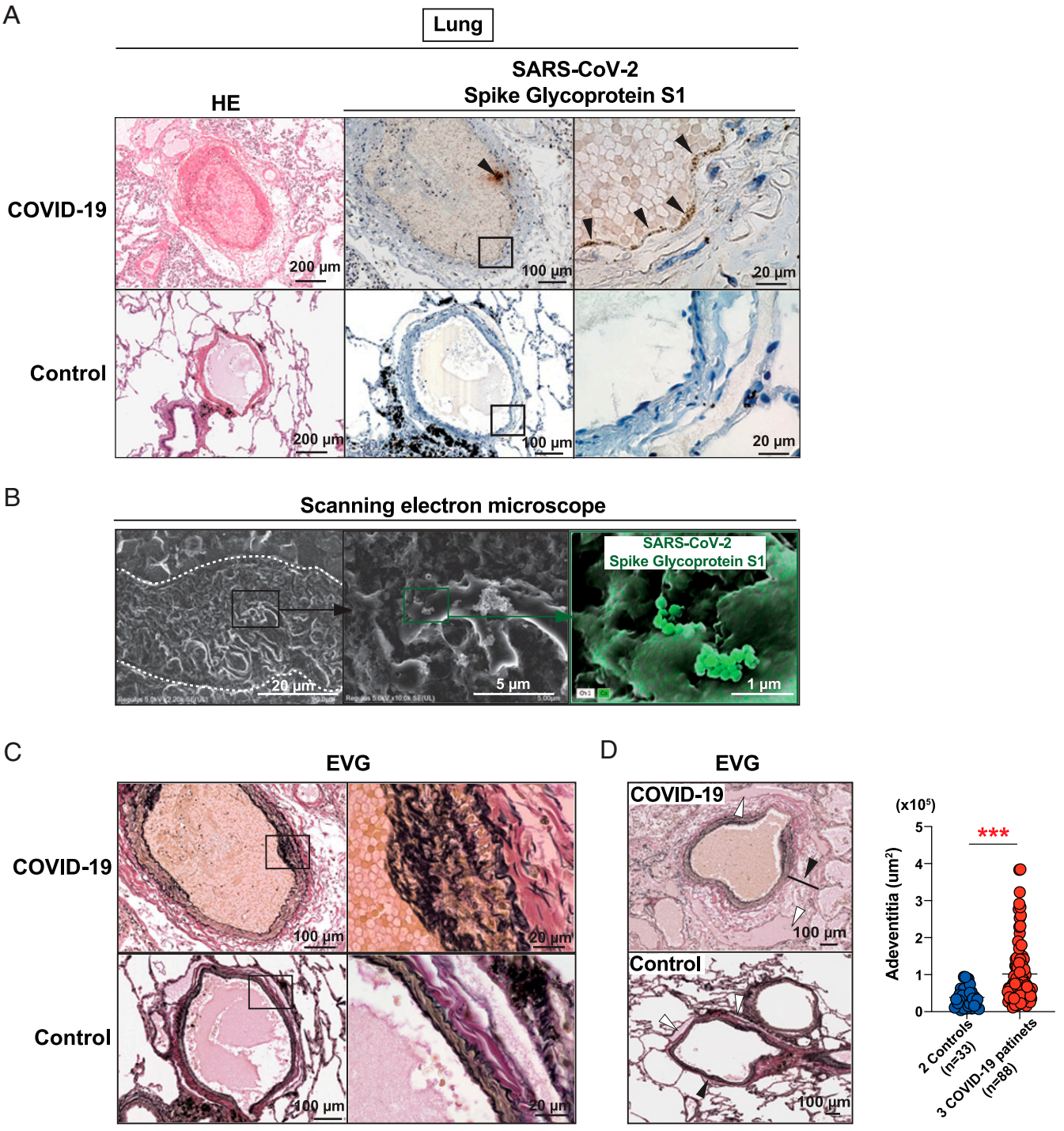

Fig. 1. Exudative vasculitis in the lung of COVID-19 patients. (*A*) Representative images of the lung of fatal COVID-19 cases and control cases who died of stomach cancer with HE staining (*Left*). Locations of SARS-CoV-2 in the lungs of fatal COVID-19 cases were determined by immunohistochemistry using anti-–SARS-CoV-2 spike glycoprotein antibody (*Center* and *Right*). SARS-CoV-2 spike glycoprotein-positive cells are indicted by black arrowheads. The inside of the open rectangles in the *Center* is magnified, *Right*. (*B*) Images of the scanning electron microscope in the area indicated by black arrowheads in the *Upper Center* image of *A*. SARS-CoV-2 viruses are shown with light green using anti–SARS-CoV-2 spike glycoprotein antibody (*Right*). (*C*) EVG staining of the lung from fatal COVID-19 cases and control cases who died with stomach cancer. Images in the open rectangles in the *Left* are magnified, *Right*. (*D*) Representative image of exudative vasculitis in the lungs of fatal COVID-19 cases and control cases who died with stomach cancer using EVG staining. White arrowheads indicate lymphatic ducts. Dimensions of adventitia (black arrowhead) of a muscular artery (100 to 500 μm) in three COVID-19 patients and two control donors were pooled (*Right*). Statistical significance was determined by the Mann–Whitney *U* test. ***$P < 0.001$.

transcriptomes of peripheral blood mononuclear cells (PBMCs) were analyzed, and uniform manifold approximation and projection (UMAP) identified 8 clusters in the PBMCs of 21 COVID-19 patients (Fig. 2*A* and *SI Appendix*, Fig. S2*A*). Fatal COVID-19 cases showed a decreased proportion of lymphoid cell clusters, such as $CD4^+$ T cells and B cells, in PBMCs compared with moderate COVID-19 cases, which was consistent with the laboratory tests (Fig. 2*B* and *SI Appendix*, Figs. S1*B* and S2*B*). In contrast, the proportion of myeloid cell clusters, including conventional and nonconventional monocytes, was increased in PBMCs of fatal COVID-19 cases compared with moderate COVID-19 cases (Fig. 2*B* and *SI Appendix*, Fig. S2*B*). A single-sample gene-set variation analysis (ssGSVA) identified the top 10 pathways accumulated in $CD45^+$ cells of fatal

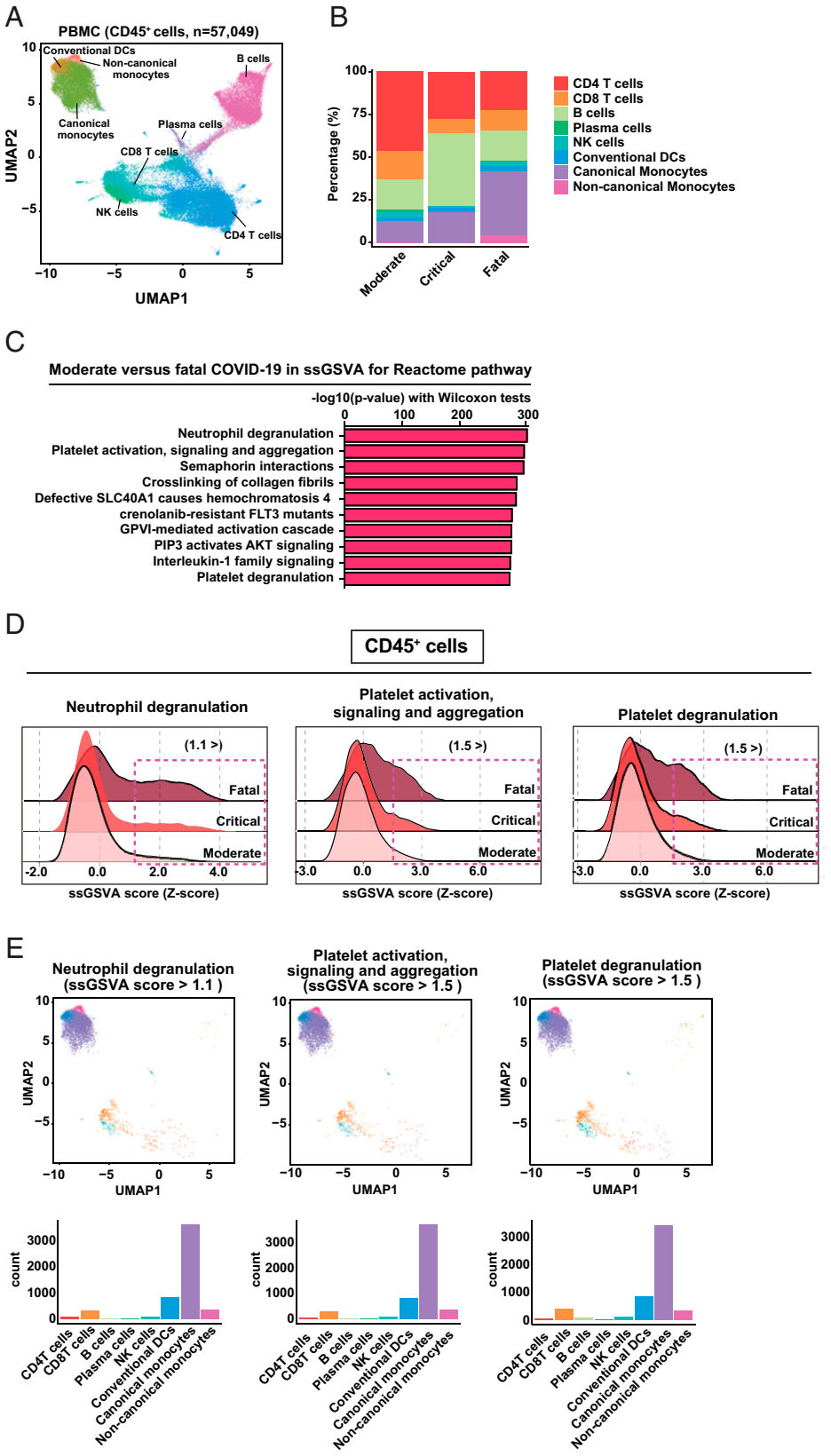

Fig. 2. A sc RNAseq analysis revealed dysregulation of myeloid cells with biased up-regulation of neutrophil and platelet activation gene sets in the blood of COVID-19 patients. (*A*) UMAP projection of CD45^{+} cells at 57,049 single-cell transcriptomes isolated from PBMCs of 21 patients (moderate $n = 10$, severe $n = 6$, fatal $n = 5$) is depicted and colored according to the 8 cellular populations. (*B*) Percentages of cell compositions in PBMCs for moderate, severe, and fatal COVID-19 cases are shown. (*C*) The bar graph shows the ssGSVA scores in pathways enriched for fatal COVID-19 cases compared with moderate COVID-19 cases. (*D*) ssGSVA scores of neutrophil degranulation (*Left*), platelet activation, signaling, and aggregation (*Center*), and platelet degranulation (*Right*) are projected on ridgeline plots. Open rectangles with dashed lines indicate higher ssGSVA scores (neutrophil degranulation: 1.1 > ssGSVA; platelet activation, signaling, and aggregation, and platelet degranulation: 1.5 > ssGSVA). (*E*) Immune cells gated by ssGSVA scores in *D* are projected on the UMAP (*Upper*) and bar plot showing the counts of each cell population (under panel).

COVID-19 cases, including "neutrophil degranulation" and platelet activation-related pathways, such as "plate activation, signaling and aggregation" and "platelet degranulation" (Fig. 2*C*). Ridge plots revealed that $CD45^+$ cells from fatal COVD-19 cases showed a higher ssGSVA score for neutrophil degranulation, platelet activation, signaling and aggregation, and platelet degranulation than those from $CD45^+$ cells from critical or moderate COVID-19 cases (Fig. 2*D*). UMAP plots drawn using the subpopulation of $CD45^+$ cells with robust activation of these pathways, which were gated in the Ridge plot (Fig. 2*D*, red-dotted rectangles), indicated that the majority of $CD45^+$ cells with high indicated ssGSVA scores were myeloid cell clusters (Fig. 2 *E*, *Upper*), specifically a subpopulation of monocytes (Fig. 2 *E*, *Lower*). Taken together, these findings indicated that circulating immune cells in critical and fatal COVID-19 cases were characterized by increased numbers of myeloid cells with biased up-regulation of platelet-activating signature.

Noncanonical Monocytes with Enhanced Expression of THBS-1 Were Accumulated in the Lungs of Fatal COVID-19. Next, we sought to identify the molecules expressed in myeloid clusters that were involved in the pathogenicity of fatal COVID-19 cases. To this end, we analyzed our scRNA-seq datasets from PBMCs of COVID-19 patients (Fig. 2*A*). $CD14^+$ myeloid cell clusters were divided into three subpopulations of canonical monocytes, noncanonical monocytes, and conventional dendritic cells (Fig. 3*A*). A total of 43 genes exhibited a >1.4-fold difference in expression between canonical and noncanonical monocytes (Fig. 3*B*). The gene encoding Thrombospondin 1 (*THBS1*) was among the most highly differentially expressed genes noncanonical monocytes and is known to promote platelet aggregation (Fig. 3*B*) (30, 31). Indeed, among the platelet activation-related pathways, such as plate activation, signaling, and aggregation and platelet degranulation, fatal COVD-19 cases showed seven up-regulated genes, including *THBS1*, compared with moderate COVID-19 cases (Fig. 3*C*). *FTL*, which encodes ferritin light chain, *RENT, ANXA2*, *S100A11*, and other genes were up-regulated in fatal COVID-19 cases among neutrophil degradation-related genes (*SI Appendix*, Fig. S3*A*). Both the UMAP plot and violin plot confirmed the enhanced expression of *THBS1* in noncanonical monocytes from fatal COVID-19 cases (Fig. 3 *D* and *E*). In contrast, *SRGN*, which encodes Serglycin, a hematopoietic proteoglycan core protein, was expressed in a variety of types of immune cells (*SI Appendix*, Fig. S3 *B* and *C*). Histological analyses of the lungs from fatal COVID-19 cases in our cohort 1 revealed the infiltration of THBS-1–expressing $CD163^+$ noncanonical monocytes around the inflammatory vessels, but the samples from control patients showed no infiltration of such a cell population (Fig. 3*F*). These results indicate that the lungs from fatal COVID-19 cases were characterized by the infiltration of noncanonical monocytes, which have the potential to induce platelet activation at local inflammatory sites.

Plasma Myl9 Levels Depicted the Severity of COVID-19. Consistent with the infiltration of noncanonical monocytes with an up-regulated platelet-activating signature in the lungs of fatal COVID-19 cases, we detected the formation of microthrombi stained by phosphotungstic acid-hematoxylin (PTAH) in arteries with exudative vasculitis of the lungs of fatal COVID-19 cases in cohort 1 (*SI Appendix*, Fig. S4*A*).

Myl9, a regulatory component of myosin protein, belongs to the myosin light chain family of molecules and has high homology with Myl12a (93%) and Myl12b (93%) in humans (32). Activated platelets release Myl9, which forms thrombus-like structures in the vasculature of patients with eosinophilic rhinosinusitis, an intractable allergic disease (33). Moreover, plasma Myl9 levels in patients with Crohn's disease were correlated with the disease severity (34). Thus, we hypothesized that vasculitis induced by SARS-CoV-2 infection-activated platelets, leading to the release of Myl9 and the generation of a net like structure. Indeed, $CD41^+$ platelets accompanied by the deposition of Myl9/12 were detected within the microthrombi in the lungs of fatal COVID-19 cases (Fig. 4*A* and *SI Appendix*, Fig. S4*B*). To test whether the plasma Myl9 level is correlated with the severity of COVID-19, we next examined the plasma Myl9 levels in our cohort 2 using an ELISA (*SI Appendix*, Fig. S1*A*). The concentration of Myl9 in the plasma of COVID-19 patients ($n = 123$) at admission to hospital was significantly higher than those in healthy controls ($n = 30$) (Fig. 4*B*, blue circles versus red circles). However, the concentration of plasma Myl9 in patients with a bacterial infection, such as sepsis ($n = 9$), and those undergoing major surgical invasion of the heart ($n = 15$) was not increased significantly (Fig. 4*B*). The receiver operating characteristics (ROC) curve of the plasma Myl9 levels revealed a high predictive value for COVID-19 patients (area under the ROC curve = 0.964, 95% confidence interval [CI] 0.933 to 0.995) (Fig. 4*C*). In the same patients, the plasma Myl9 levels at discharge were significantly lower than those at admission (Fig. 4*D*), and also lower than the maximum Myl9 values during hospitalization (*SI Appendix*, Fig. S4*C*). However, some patients with fatal disease showed higher levels of Myl9 when they died in comparison to the levels at admission (Fig. 4*D*).

To investigate whether the severity of COVID-19 is correlated with the plasma Myl9 levels, the patients were classified according to the disease severity of COVID-19 (*SI Appendix*, Table S1). Both severe and critical cases ($n = 24$ and $n = 27$, respectively) showed elevated plasma Myl9 concentrations in comparison to moderate cases, even after adjustment according to sex and age ($n = 60$) (Fig. 4*E*). Fatal cases ($n = 12$) exhibited the highest plasma Myl9 concentrations among the four categories of disease severity (Fig. 4*E*). We next examined the correlations of plasma Myl9 levels with other laboratory data (Fig. 4*F* and *SI Appendix*, Fig. S4 *D–F*). The plasma Myl9 levels were positively correlated with the numbers of neutrophils ($P < 0.0001$, $r = 0.742$) and white blood cells ($P < 0.0001$, $r = 0.742$) and the level of LDH ($P < 0.0001$, $r = 0.575$), IL-8 ($P < 0.0001$, $r = 0.500$), and D-dimer ($P < 0.0001$, $r = 0.466$) (Fig. 4*F* and *SI Appendix*, Fig. S4 *D* and *E*). Thus, the plasma Myl9 level of COVID-19 patients at admission are able to distinguish patients with severe, critical, and fatal disease from those with moderate disease, similarly to other blood biomarkers (*SI Appendix*, Fig. S4*F*). Plasma Myl9 levels at admission were also positively correlated with the duration of hospitalization ($P < 0.0001$, $r = 0.484$) (Fig. 4*G*). Furthermore, a multivariate logistic regression analysis revealed that the odds ratio of Myl9 was 1.962 (95% CI, 1.465 to 2.628), suggesting that the plasma Myl9 level was associated with a risk of requiring oxygen supplementation (score ≥ 5) at 7 d after admission (*SI Appendix*, Fig. S4*G*).

Moreover, we found that patients who received anti–IL-6 antibody treatment showed a greater reduction of plasma Myl9 in comparison to patients who did not receive anti–IL-6 antibody treatment (*SI Appendix*, Fig. S4*H*). Based on reports that autoantibodies to type I IFNs or genetic defects in type I IFN signaling can be a major risk factor underlying life-threatening disease in patients with COVID-19 (7–10), we measured the plasma anti–IFN-α2 antibody levels and found that seven cases had antibodies. The levels of plasma Myl9 at admission in

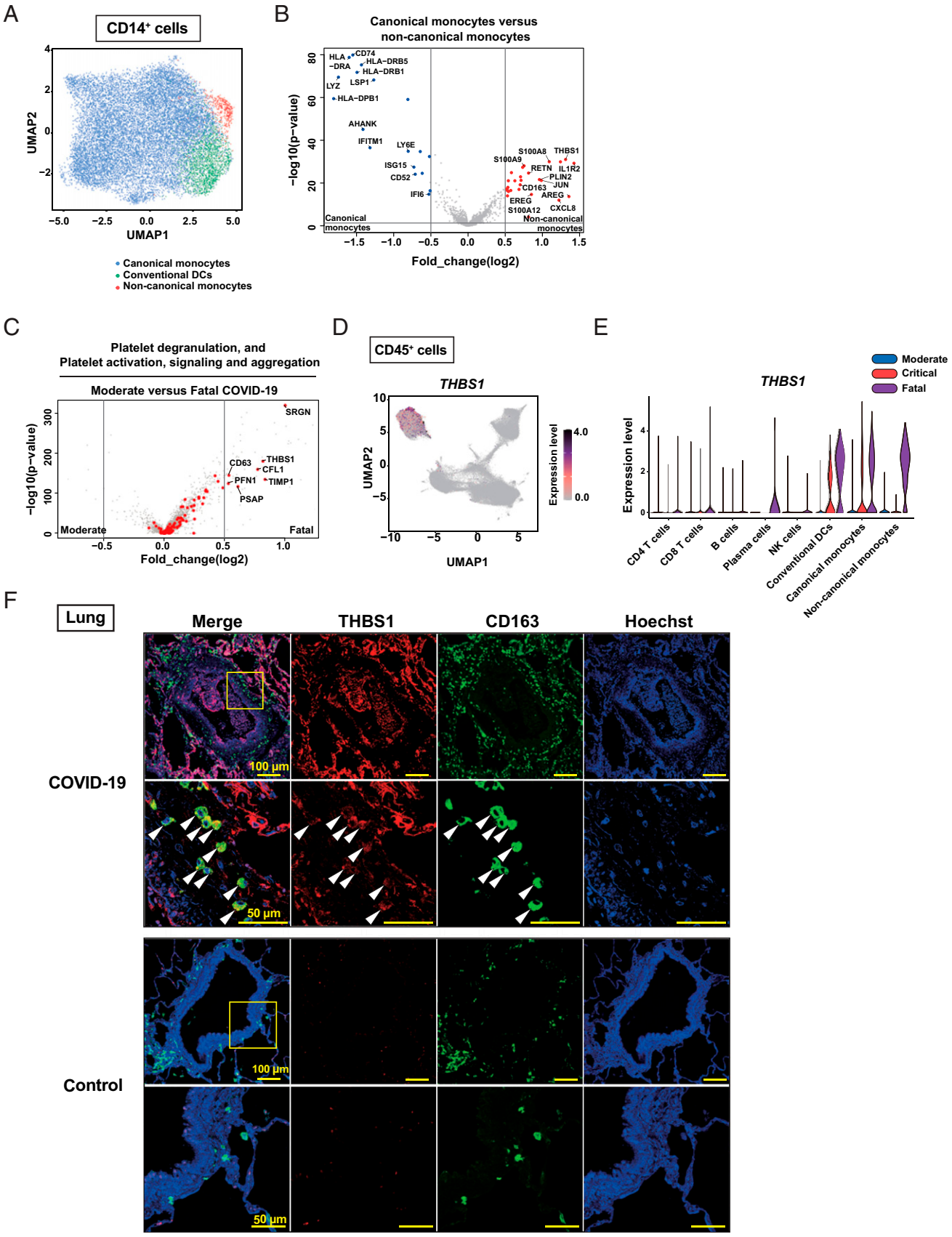

Fig. 3. Noncanonical monocytes expressing THBS-1 were accumulated in the lung of COVID-19 patients. (*A*) The UMAP projection of CD14^{+} cells from moderate, severe, and critical COVID-19 cases is depicted and colored according to the cellular populations. DC, dendritic cell. (*B*) The volcano plot depicts the differential gene expression of noncanonical monocytes in comparison to canonical monocytes. (*C*) The volcano plot depicts the differential gene expressions related to platelet degranulation, activation, signaling, and aggregation between moderate and fatal COVID-19 cases. (*D*) The UMAP shows the expression of THBS-1 with color intensity. (*E*) Violin plots show the distribution of THBS-1 in each cell population of moderate, critical, and fatal COVID-19 cases. (*F*) Identification of noncanonical macrophages expressing CD163, and THBS-1 in the peripheral lung tissue of the fatal COVID-19 case (case #1) and control case who died of stomach cancer. The inside of the open rectangles in the *Upper* panels is magnified in the *Lower* panels, respectively.

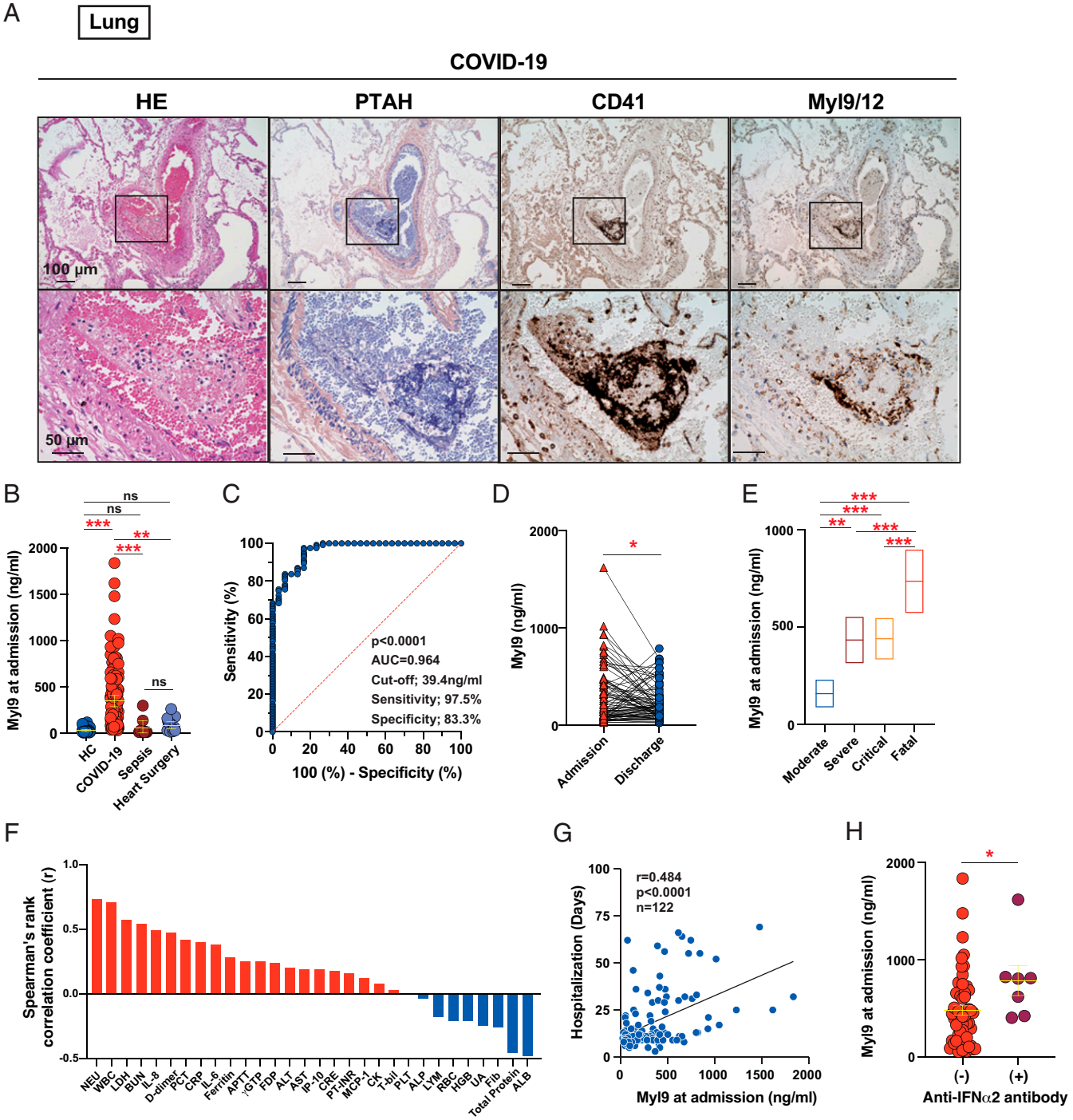

Fig. 4. Plasma Myl9, a component of the thrombus, indicates the severity of COVID-19. (*A*) HE and PTAH staining of the peripheral lung tissue from the fatal COVID-19 case (case #1). Brown staining developed by immunohistochemistry indicates platelets (CD41) or Myl9 deposition in the thrombus. (*B*) Plasma Myl9 levels from healthy controls (HC, $n = 30$), COVID-19 patients at admission ($n = 123$), sepsis patients at admission ($n = 9$), and heart surgery patients on the day when surgery was performed ($n = 15$). Yellow lines indicate mean values and 95% CIs. Comparisons were performed by the Kruskal–Wallis test. ns, not significant; $^{**}P < 0.001$; $^{***}P < 0.0001$. (*C*) ROC curve for plasma Myl9 levels between COVID-19 patients and healthy controls. (*D*) Plasma Myl9 levels in the COVID-19 patients at admission and at discharge ($n = 87$). The same patients are connected via lines. The comparison was performed by a paired *t* test. $^{*}P < 0.05$. (*E*) A multiple linear regression analysis was performed to evaluate the association between Myl9 and severity (moderate, $n = 60$; severe, $n = 24$; critical, $n = 27$; fatal, $n = 12$). $^{**}P < 0.001$; $^{***}P < 0.0001$. (*F*) Correlation of levels of plasma Myl9 and each blood marker using Spearman's correlation coefficient (r). All blood samples from COVID-19 patients during hospitalization were analyzed. (*G*) Correlation between plasma Myl9 levels and days after admission in COVID-19 patients. Individual data were adjusted by age and sex. Tukey's method was applied for pairwise group comparisons. (*H*) Plasma Myl9 levels at admission when patients with severe, critical, and fatal disease were divided according to the presence of anti–IFN-α2 antibodies (anti–IFN-α2 antibody [−], $n = 56$; [+] $n = 7$). The comparison was performed by a paired *t* test. $^{*}P < 0.05$. The values indicate the mean ± SEM.

patients with severe, critical, and fatal disease with anti–IFN-α2 antibodies were higher than those in patients without the antibodies (Fig. 4*H*). In contrast, the presence of hypertension or obesity did not significantly affect the plasma Myl9 levels in COVID-19 patients with severe, critical, or fatal disease (*SI Appendix*, Fig. S4*I*). In addition, some correlation ($r = 0.294$) was found between age and the plasma Myl9 level in severely ill patients (*SI Appendix*, Fig. S4*J*).

These results indicate that the plasma Myl9 level reflects the patient clinical condition and may provide an objective diagnosis of the severity of COVID-19.

Discussion

This study presents evidence that exudative vasculitis accompanied by the accumulation of SARS-CoV-2 in the arteries of the lungs develops in fatal COVD-19. Abnormal myeloid subsets, especially noncanonical monocytes with enhanced expression of THBS-1 are accumulated in the lungs of fatal COVID-19 cases. The plasma Myl9 level reflects the clinical condition of COVID-19 patients and may predict their disease severity.

Endothelial injury and pathological changes such as microthrombi within blood vessels, have been well described in the lungs of COVID-19 patients (35). Our histopathology analysis of lung tissue from fatal COVID-19 cases additionally identified a massive exudative inflammation in the pulmonary interstitium in COVID-19 patients. Indeed, the arteries of the lungs of all fatal COVID-19 cases had ruptured and thickened elastic fibers accompanied by dilated adventitia, which are characteristic histological changes of exudative vasculitis. However, the typical features of exudative vasculitis were not detected in the kidneys. Additional studies with a large number of autopsy cases are required to determine whether the vasculitis in COVID-19 patients is local or systemic. Ultrastructural analyses using FE-SEM with EDX showed the aggregation of SARS-CoV-2 particles in the tunica media and destruction of the tunica media of lung vessels. Destruction of the smooth muscle layer may then cause to leakage of intravascular plasma into the interstitial space and COVID-19 pneumonia with severe respiratory dysfunction. Furthermore, leaking platelets from the injured vessels are likely activated by collagens in the outer membrane of blood vessels, which causes the elevation of plasma Myl9 in COVID-19 patients.

Increased evidence has shown that COVID-19 mortality is strongly correlated with the pulmonary vascular pathology, such as immunothrombosis and vasculitis (20, 36). Consistent with previous reports, we also detected microthrombi in the arteries with exudative vasculitis in the lungs of fatal COVD-19 cases. Early reports on the pathology of COVID-19 suggested that direct SARS-CoV-2 infection of the vascular endothelium might induce vascular injury and thrombosis (37, 38). However, the direct viral infection of the vascular endothelium has been controversial in light of several experimental results, including the low expression of angiotensin converting enzyme-2 (ACE-2) on the vascular endothelial cells (21). Instead of direct vascular injury, excessive immune responses by SARS-CoV-2 infection may indirectly damage vascular endothelial cells (39, 40). However, the causes for the overreaction of the immune system specifically around the vessels have remained uncertain. In the present study, we clearly demonstrated the aggregation of SARS-CoV-2 particles in the extracellular spaces of the arteries in the inflamed lungs of fatal COVID-19 cases using an FE-SEM with EDX system. The presence of SARS-CoV-2 particles in the vessel membrane suggests a direct pathogenic role of SARS-CoV-2. Furthermore, the aggregation of SARS-CoV-2 in the extracellular spaces of the vessel wall may activate local host immunity, which triggers the inflammation of vessels, thereby causing exudative vasculitis accompanied by the induction of immunothrombosis in the arteries. However, no patients who were enrolled in the study showed any clinical symptoms of thrombotic events before or after their hospitalization. One of the possible reasons is that patients with elevated D-dimer levels were treated with anticoagulants for the prevention of thrombotic events.

The pathogenic roles of neutrophil activation and neutrophil-derived extracellular traps (NETs) in the immunothrombosis in COVID-19 patients have been elucidated (41–44). SARS-CoV-2 directly stimulates neutrophils to release NETs in an ACE-2–dependent manner (41). NETs are involved in the pathogenesis of immune thrombosis in various organs, such as the lung and the heart, in COVID-19 patients (42, 43). In fact, scRNA-seq of PBMCs from COVID-19 in our cohort 2 showed the up-regulation of the neutrophil degranulation pathway in fatal COVID-19 cases (Fig. 2 *C* and *D* and *SI Appendix*, Fig. S3*A*). The neutrophil degranulation-related genes that were up-regulated in COVID-19 patients with fatal disease included *RETN* and *S100A11*, which are reported as characteristic molecules of severe disease (*SI Appendix*, Fig. S3*A*) (45, 46). Another up-regulated gene, *ANXA2*, is associated not only with binding and internalization of viruses, such as SARS-CoV-2, but also with hypofibrinolysis, which is a risk factor for venous thromboembolism (47). Therefore, excessive neutrophil activation in COVID-19 patients with severe disease may be involved in the formation of microthrombi as well as NETs. Furthermore, our scRNA-seq datasets revealed the appearance of dysregulated myeloid cells with biased up-regulation of platelet-activating signature in critical and fatal COVID-19 cases. We identified a unique subpopulation of monocytes that specifically expressed THBS-1, which is a homotrimeric multidomain glycoprotein controlling platelet-endothelial cell interactions and supporting platelet adhesion (48). THBS-1 also contributes to von Willebrand factor-dependent thrombus formation (49). Importantly, THBS-1 was specifically up-regulated in the lungs of fatal COVD-19 cases but not in the lungs of fatal influenza A cases (38). Plasma THBS-1 levels were reported to be significantly elevated in COVID-19 patients compared with healthy controls (50). Indeed, we found that noncanonical monocytes with a high expression of THBS-1 specifically appeared in the PBMCs of fatal COVID-19 cases in our cohort 2. Furthermore, THBS-1-expressing $CD163^{+}$ monocytes had infiltrated at the local inflammatory sites in fatal COVID-19 cases in our cohort 1. Taken together, these present and previous findings indicate that THBS-1 is involved in the microthrombus formation in COVID-19.

Myl9, which is a regulatory component of myosin protein and belongs to the myosin light chain family of molecules, is a functional ligand of CD69 that is highly expressed by activated leukocytes (32, 33). In the inflamed lung, activated platelets release Myl9/12, which forms the net-like structure inside of the vessel, where activated leukocytes can migrate to the local inflammatory site via CD69-Myl9 binding, thereby causing the exacerbation of inflammation (33). Importantly, treatment with either anti-CD69 or anti-Myl9/12 antibodies ameliorates airway inflammation or inflammatory bowel disease by inhibiting the infiltration of $CD69^{+}$-activated immune cells into the inflammatory tissues, suggesting that Myl9 is a therapeutic target in inflammatory diseases (33, 34). In the case of SARS-CoV-2 infection, we detected Myl9/12-expressing platelets within the microthrombi in the arteries of the lungs from fatal COVID-19 cases. A prospective study using COVID-19 plasma in our cohort 2 revealed a significant correlation between the plasma Myl9 level and the severity of COVID-19 (Fig. 4*E*). In addition, the Myl9 level at admission was correlated with the duration of hospitalization and the risk of requiring oxygen supplementation at 7 d after administration (Fig. 4*G* and *SI Appendix*, Fig. S4*G*). Thus, plasma Myl9 can be a useful biomarker to predict the future severity of COVID-19, and the measurement of Myl9 may allow us to detect patients with a high risk of becoming critically ill. Moreover, patients who received anti–IL-6 antibody treatment showed a greater reduction

of plasma Myl9 (*SI Appendix*, Fig. S4*H*), which indicates the clinical utility of plasma Myl9 for determining the efficacy of antiinflammatory treatments. We also found that patients who had anti–IFN-α2 autoantibody showed higher levels of plasma Myl9 compared with patients without anti–IFN-α2 autoantibody (Fig. 4*H*). However, further study will be needed to determine whether the anti–IFN-α2 has neutralizing activity. Furthermore, we did not test for autoantibodies against IFN-β or IFN-ω.

After SARS-CoV-2 infection, the Myl9 level may increase earlier than other blood markers. For example, we and others showed that D-dimer, a useful biomarker for the assessment of coagulation status, is important to evaluate the severity of COVID-19 (51). An increase of D-dimer indicates the presence of thrombi that were already formed in the blood vessels because it is a degradation product after fibrin formation (52). In contrast, Myl9 is released from platelets into the blood stream immediately after the activation (33). Therefore, measurement of plasma Myl9 levels may allow us to detect the early stage of thrombus formation. Furthermore, the level of Myl9 is specifically associated with hyperactivation of platelets. Other biomarkers, including CRP, are elevated in patients with various types of inflammation, including bacterial infection and sterile inflammation (Fig. 4*B*). Indeed, an increase in plasma Myl9 levels was not detected in patients with bacterial infections, such as sepsis, or patients with surgical invasion (Fig. 4*B*). These results indicate that the local activation of platelets in the lung causes Myl9 release, resulting in high concentrations of systemic Myl9 in the plasma of COVID-19 patients, but the local activation of platelets may not be induced in patients with bacterial infection or surgical invasion. Taken together, our findings suggest that plasma Myl9 may be a useful biomarker that has the potential to identify the severity of COVID-19 at the initial assessment in the hospital, leading to the provision of optimal medical treatments to patients with high plasma Myl9 levels. Considering that the increase of plasma Myl9 suggests the presence of vasculitis in the body, it may be possible to diagnose other types of vasculitis, such as multisystem inflammatory syndrome in children (MIS-C), which causes Kawasaki disease-like vasculitis in pediatric patients (53). Furthermore, accumulating Myl9 in the arteries in the lung may be a novel therapeutic target for COVID-19 to prevent the infiltration of activated inflammatory leukocytes into the local inflamed tissue.

In summary, we found that SARS-CoV-2 infection caused exudative vasculitis accompanied by SARS-CoV-2 elements in the blood vessels in the lung of COVID-19 patients with fatal disease. The accumulation of THBS-1–expressing noncanonical monocytes around the affected vessels may contribute to the formation of Myl9-containg microthrombi by promoting platelet aggregation. Platelet activation by vascular injury or THBS-1 may result in increased plasma Myl9 levels in COVID-19 patients (*SI Appendix*, Fig. S5). We found that the plasma Myl9 level reflects the clinical condition of COVID-19 patients. Thus, plasma Myl9 will be a biomarker to predict the severity of COVID-19, and a potential therapeutic target for preventing microthrombosis and intractable vasculitis in COVID-19.

Materials and Methods

Study Participants. From late July 2020 to March 2021, a total of 123 patients who were confirmed by RT-PCR to have been infected with SARS-CoV-2 were included in the study. The inclusion criteria were age over 20 y old, with no specific exclusion criteria aside from the age. Blood samples were obtained from healthy subjects ($n = 30$), sepsis patients ($n = 9$), or heart surgery patients ($n = 15$) as control groups for COVID-19. We retrospectively evaluated and analyzed the detailed medical history, physical examination findings, and hematological and biochemical evaluation results obtained from those patients. Blood samples were collected using EDTA-2Na blood collection tubes once every week for moderate cases or two to three times per week for severe or critical cases.

These studies were approved by the ethics committee of the Chiba University Hospital (HS202005-01) and the ethics committee of Graduate School of Medicine, Chiba University (#959). The autopsy samples were collected under a protocol approved by the ethics committee of Graduate School of Medicine, Chiba University (M10040). Written informed consent was provided by each participant or their family before the study.

Clinical Classifications and Complication Definitions. Patients were classified for COVID-19 severity by physicians according to the clinical status described in the WHO R&D Blueprint, novel Coronavirus, COVID-19 therapeutic trial synopsis (2020) (54) (Table 1). We followed the previous reports for the severity scoring system and the severity classification (24, 25). In brief, the classifications of COVID-19 by clinical status are as follows: Moderate cases, who are patients not requiring oxygen supplementation and medical care (score 3), and patients not requiring oxygen supplementation, but requiring medical care (score 4); severe cases, who are patients requiring low-flow oxygen supplementation (score 5); and critical cases, who are patients requiring high-flow oxygen devices (score 6), and patients admitted to the intensive-care unit and requiring a mechanical ventilator or extracorporeal membrane oxygenation (score 7).

Detailed descriptions of all materials and methods are provided in *SI Appendix*, *SI Materials and Methods*.

Data Availability. All study data are included in the article and *SI Appendix*. Additional data is available at the Gene Expression Omnibus at accession number GSE208337 (55) .

ACKNOWLEDGMENTS. We thank Takashi Yoshida (Juntendo University Faculty of Medicine and Graduate School of Medicine), Yoshifumi Suzuki (Juntendo University Faculty of Medicine and Graduate School of Medicine), Ryogo Ema (Eastern Chiba Medical Center), and Rintaro Nishimura (Eastern Chiba Medical Center) for their support in performing sample acquisition; Toshiro Masuda and Haruna Ebisu for managing this clinical study; Mr. Shintaro Hishiyama (BRUKER) for technical assistance on energy-dispersive X-ray spectroscopy analysis; Mrs. Mika Hashimoto (Advanced Institute of Science and Technology) for technical assistance on histological analysis using immunofluorescence detection; and Damon Tumes for his careful reading and valuable suggestions. This work was supported by grants from the following: the Ministry of Education, Culture, Sports, Science and Technology (MEXT Japan) Grants-in-Aid for Scientific Research (S) JP19H05650, (B) 20H03685, (C) 19K16683, 20K08769, 22K15485, and 22K15484, Transformative Research Areas (B) JP21H05120 and JP21H05121; the Practical Research Project for Allergic Diseases and Immunology (Research on Allergic Diseases and Immunology) from the Japan Agency for Medical Research and Development (AMED) (JP21ek0410060 and JP21ek0410082); the Program to Develop Countermeasure Technologies against Viral and Other Infectious Diseases, AMED (JP20he0622037); AMED-Programs for Medical Intervention (JP20gm6110005); AMED-Core Research for Evolutionary Science and Technology (JP21gm1210003); AMED-Advanced Measurement and Analysis Systems project (JP19hm0102069h001); the Japan Science and Technology Agency (JST) Fusion Oriented REsearch for disruptive Science and Technology (FOREST) Project (JPMJFR200R); JST-Moonshot R&D (JPMJMS2025), and by the Mochida Memorial Foundation for Medical and Pharmaceutical Research; the MSD Life Science Foundation; Kowa Life Science Foundation; and the Takeda Science Foundation.

Author affiliations: [a]Department of Immunology, Graduate School of Medicine, Chiba University, Chiba 260-8670, Japan; [b]Department of Pathology, Graduate School of Medicine, Chiba University, Chiba 260-8670, Japan; [c]Department of Emergency and Critical Care Medicine, Graduate School of Medicine, Chiba University, Chiba 260-8670, Japan; [d]Clinical Research Center, Chiba University Hospital, Chiba 260-8677, Japan; [e]Department of Respiratory Medicine, Juntendo University Faculty of Medicine and Graduate School of Medicine, Tokyo 113-8431, Japan; [f]Department of Respiratory Medicine, Funabashi Central Hospital, Chiba 273-8556, Japan; [g]Department of

Infectious Diseases, Japanese Red Cross Narita Hospital, Chiba 286-0041, Japan; [h]Department of Respiratory Medicine, Eastern Chiba Medical Center, Chiba 283-8686, Japan; [i]Department of Anesthesiology and Critical Care Medicine, School of Medicine, Fujita Health University, Aichi 470-1192, Japan; [j]Department of Pathology, School of Medicine, Fujita Health University, Aichi 470-1192, Japan; [k]Department of Respirology, Funabashi Municipal Medical CenterChiba 273-8588, Japan; [l]Department of Respirology, Kimitsu Chuo Hospital, Chiba 292-0822, Japan; [m]Department of Gastroenterology, National Hospital Organization Chiba Medical Center, Chiba 260-8606, Japan; [n]Department of Respirology, Graduate School of Medicine, Chiba University, Chiba 260-8670, Japan; [o]Department of Pathology, Asahi General Hospital, Chiba 289-2511, Japan; [p]Department of Surgical Pathology, Sapporo Medical University of Medicine, Sapporo 060-8543, Japan; [q]Department of Gastroenterology and Hepatology, Sapporo Medical University of Medicine, Sapporo 060-8543, Japan; [r]DLC Research Institute LLC, Nagasaki 850-0011, Japan; [s]CNT-Application Research Center, National Institute of Advanced Industrial Science and Technology, Tsukuba 305-8565, Japan; [t]Department of Experimental Immunology, Graduate School of Medicine, Chiba University, Chiba 260-8670, Japan; [u]Department of General Thoracic Surgery, Graduate School of Medicine, Chiba University, Chiba 260-8670, Japan; [v]Department of Infectious Diseases, Chiba University Hospital, Chiba 260-8677, Japan; [w]COVID-19 Vaccine Center, Chiba University Hospital, Chiba 260-8677, Japan; [x]Department of Allergy and Clinical Immunology, Graduate School of Medicine, Chiba University, Chiba 260-8670, Japan; [y]Cellular and Molecular Biotechnology Research Institute, National Institute of Advanced Industrial Science and Technology, Tsukuba 305-8565, Japan; [z]Department of Endocrinology, Hematology, and Gerontology, Graduate School of Medicine, Chiba University, Chiba 260-8670, Japan; and [aa]Core Research for Evolutionary Science and Technology, Japan Agency for Medical Research and Development, Chiba 260-8670, Japan

Author contributions: C.I., K.H., M.K., and T. Nakayama designed research; C.I., M.K., S. Ikehara, K.A., T. Shimada, S. Kuriyama, S.O., E.Y., A.A., K.K., R. Hirasawa, T. Hishiya, K. Tsuji, T. Nagaoka, S. Ishikawa, A.K., H.M., R. Hase, Y.K., N.K., T.T., S.N., T.U., S. Kaneda, S.S., M. Tobiume, Y. Suzuki, M. Tsujiwaki, T.K., T. Hasegawa, H. Nakase, O.N., K. Takahashi, K.B., Y. Iizumi, T.O., I.Y., H.I., H. Nakajima, T. Suzuki, T.-a.N., Y. Ikehara, and K.Y. performed research; C.I., K.H., Y. Inaba, Y. Shiko, M.Y.K., H.H., Y. Ikehara, and T. Nakayama analyzed data; and C.I., K.H., and T. Nakayama wrote the paper.

The authors declare no competing interest.

1. P. A. Mudd *et al.*, Distinct inflammatory profiles distinguish COVID-19 from influenza with limited contributions from cytokine storm. *Sci. Adv.* **6**, eabe3024 (2020).
2. M. Patone *et al.*, Mortality and critical care unit admission associated with the SARS-CoV-2 lineage B.1.1.7 in England: An observational cohort study. *Lancet Infect. Dis.* **21**, 1518–1528 (2021).
3. COVID-19 Forecasting Team, Variation in the COVID-19 infection-fatality ratio by age, time, and geography during the pre-vaccine era: A systematic analysis. *Lancet* **399**, 1469–1488 (2022).
4. F. Zhou *et al.*, Clinical course and risk factors for mortality of adult inpatients with COVID-19 in Wuhan, China: A retrospective cohort study. *Lancet* **395**, 1054–1062 (2020).
5. S. S. Bhopal, R. Bhopal, Sex differential in COVID-19 mortality varies markedly by age. *Lancet* **396**, 532–533 (2020).
6. W. Jassat *et al.*; DATCOV author group, Risk factors for COVID-19-related in-hospital mortality in a high HIV and tuberculosis prevalence setting in South Africa: A cohort study. *Lancet HIV* **8**, e554–e567 (2021).
7. P. Bastard *et al.*; HGID Lab; COVID Clinicians; COVID-STORM Clinicians; NIAID Immune Response to COVID Group; NH-COVAIR Study Group; Danish CHGE; Danish Blood Donor Study; St. James's Hospital; SARS CoV2 Interest group; French COVID Cohort Study Group; Imagine COVID-Group; Milieu Intérieur Consortium; CoV-Contact Cohort; Amsterdam UMC Covid-19; Biobank Investigators; COVID Human Genetic Effort; CONSTANCES cohort; 3C-Dijon Study; Cerba HealthCare; Etablissement du Sang study group, Autoantibodies neutralizing type I IFNs are present in ∼4% of uninfected individuals over 70 years old and account for ∼20% of COVID-19 deaths. *Sci. Immunol.* **6**, eabl4340 (2021).
8. P. Bastard *et al.*; HGID Lab; NIAID-USUHS Immune Response to COVID Group; COVID Clinicians; COVID-STORM Clinicians; Imagine COVID Group; French COVID Cohort Study Group; Milieu Intérieur Consortium; CoV-Contact Cohort; Amsterdam UMC Covid-19 Biobank; COVID Human Genetic Effort, Autoantibodies against type I IFNs in patients with life-threatening COVID-19. *Science* **370**, 423 (2020).
9. Q. Zhang, P. Bastard, A. Cobat, J. L. Casanova; COVID Human Genetic Effort, Human genetic and immunological determinants of critical COVID-19 pneumonia. *Nature* **603**, 587–598 (2022).
10. Q. Zhang *et al.*; COVID-STORM Clinicians; COVID Clinicians; Imagine COVID Group; French COVID Cohort Study Group; CoV-Contact Cohort; Amsterdam UMC Covid-19 Biobank; COVID Human Genetic Effort; NIAID-USUHS/TAGC COVID Immunity Group, Inborn errors of type I IFN immunity in patients with life-threatening COVID-19. *Science* **370**, 422 (2020).
11. K. Uriu *et al.*; Genotype to Phenotype Japan (G2P-Japan) Consortium, Neutralization of the SARS-CoV-2 Mu variant by convalescent and vaccine serum. *N. Engl. J. Med.* **385**, 2397–2399 (2021).
12. J. Hadjadj *et al.*, Impaired type I interferon activity and inflammatory responses in severe COVID-19 patients. *Science* **369**, 718–724 (2020).
13. J. J. Manson *et al.*, COVID-19-associated hyperinflammation and escalation of patient care: A retrospective longitudinal cohort study. *Lancet Rheumatol.* **2**, e594–e602 (2020).
14. C. Lucas *et al.*; Yale IMPACT Team, Longitudinal analyses reveal immunological misfiring in severe COVID-19. *Nature* **584**, 463–469 (2020).
15. D. Mathew *et al.*; UPenn COVID Processing Unit, Deep immune profiling of COVID-19 patients reveals distinct immunotypes with therapeutic implications. *Science* **369**, eabc8511 (2020).
16. T. Takahashi *et al.*; Yale IMPACT Research Team, Sex differences in immune responses that underlie COVID-19 disease outcomes. *Nature* **588**, 315–320 (2020).
17. M. Liao *et al.*, Single-cell landscape of bronchoalveolar immune cells in patients with COVID-19. *Nat. Med.* **26**, 842–844 (2020).
18. P. A. Szabo *et al.*, Longitudinal profiling of respiratory and systemic immune responses reveals myeloid cell-driven lung inflammation in severe COVID-19. *Immunity* **54**, 797–814.e6 (2021).
19. F. D'Agnillo *et al.*, Lung epithelial and endothelial damage, loss of tissue repair, inhibition of fibrinolysis, and cellular senescence in fatal COVID-19. *Sci. Transl. Med.* **13**, eabj7790 (2021).
20. D. McGonagle, C. Bridgewood, A. V. Ramanan, J. F. M. Meaney, A. Watad, COVID-19 vasculitis and novel vasculitis mimics. *Lancet Rheumatol.* **3**, e224–e233 (2021).
21. R. F. Nicosia, G. Ligresti, N. Caporarello, S. Akilesh, D. Ribatti, COVID-19 vasculopathy: Mounting evidence for an indirect mechanism of endothelial injury. *Am. J. Pathol.* **191**, 1374–1384 (2021).
22. J. Helms *et al.*; CRICS TRIGGERSEP Group (Clinical Research in Intensive Care and Sepsis Trial Group for Global Evaluation and Research in Sepsis), High risk of thrombosis in patients with severe SARS-CoV-2 infection: A multicenter prospective cohort study. *Intensive Care Med.* **46**, 1089–1098 (2020).
23. M. Levi, J. Thachil, T. Iba, J. H. Levy, Coagulation abnormalities and thrombosis in patients with COVID-19. *Lancet Haematol.* **7**, e438–e440 (2020).
24. C. D. Spinner *et al.*; GS-US-540-5774 Investigators, Effect of remdesivir vs standard care on clinical status at 11 days in patients with moderate COVID-19: A randomized clinical trial. *JAMA* **324**, 1048–1057 (2020).
25. A. H. Attaway, R. G. Scheraga, A. Bhimraj, M. Biehl, U. Hatipoğlu, Severe covid-19 pneumonia: Pathogenesis and clinical management. *BMJ* **372**, n436 (2021).
26. R. Chen *et al.*, Cytokine storm: The primary determinant for the pathophysiological evolution of COVID-19 deterioration. *Front. Immunol.* **12**, 589095 (2021).
27. J. M. Aranjani, A. Manuel, H. I. Abdul Razack, S. T. Mathew, COVID-19-associated mucormycosis: Evidence-based critical review of an emerging infection burden during the pandemic's second wave in India. *PLoS Negl. Trop. Dis.* **15**, e0009921 (2021).
28. M. Hoenigl *et al.*; ECMM and ISHAM collaborators, The emergence of COVID-19 associated mucormycosis: A review of cases from 18 countries. *Lancet Microbe* **3**, e543–e552 (2022).
29. T. Horiguchi *et al.*, Fatal disseminated mucormycosis associated with COVID-19. *Respirol. Case Rep.* **10**, e0912 (2022).
30. P. B. Narasimhan, P. Marcovecchio, A. A. J. Hamers, C. C. Hedrick, Nonclassical monocytes in health and disease. *Annu. Rev. Immunol.* **37**, 439–456 (2019).
31. W. Roberts, S. Magwenzi, A. Aburima, K. M. Naseem, Thrombospondin-1 induces platelet activation through CD36-dependent inhibition of the cAMP/protein kinase A signaling cascade. *Blood* **116**, 4297–4306 (2010).
32. M. Y. Kimura *et al.*, Crucial role for CD69 in allergic inflammatory responses: CD69-Myl9 system in the pathogenesis of airway inflammation. *Immunol. Rev.* **278**, 87–100 (2017).
33. K. Hayashizaki *et al.*, Myosin light chains 9 and 12 are functional ligands for CD69 that regulate airway inflammation. *Sci. Immunol.* **1**, eaaf9154 (2016).
34. M. Yokoyama *et al.*, Myosin light chain 9/12 regulates the pathogenesis of inflammatory bowel disease. *Front. Immunol.* **11**, 594297 (2021).
35. J. Loo, D. A. Spittle, M. Newnham, COVID-19, immunothrombosis and venous thromboembolism: Biological mechanisms. *Thorax* **76**, 412–420 (2021).
36. S. E. Fox *et al.*, Pulmonary and cardiac pathology in African American patients with COVID-19: An autopsy series from New Orleans. *Lancet Respir. Med.* **8**, 681–686 (2020).
37. Z. Varga *et al.*, Endothelial cell infection and endotheliitis in COVID-19. *Lancet* **395**, 1417–1418 (2020).
38. M. Ackermann *et al.*, Pulmonary vascular endothelialitis, thrombosis, and angiogenesis in Covid-19. *N. Engl. J. Med.* **383**, 120–128 (2020).
39. D. C. Fajgenbaum, C. H. June, Cytokine storm. *N. Engl. J. Med.* **383**, 2255–2273 (2020).
40. S. Kang *et al.*, IL-6 trans-signaling induces plasminogen activator inhibitor-1 from vascular endothelial cells in cytokine release syndrome. *Proc. Natl. Acad. Sci. U.S.A.* **117**, 22351–22356 (2020).
41. F. P. Veras *et al.*, SARS-CoV-2-triggered neutrophil extracellular traps mediate COVID-19 pathology. *J. Exp. Med.* **217**, e20201129 (2020).
42. E. A. Middleton *et al.*, Neutrophil extracellular traps contribute to immunothrombosis in COVID-19 acute respiratory distress syndrome. *Blood* **136**, 1169–1179 (2020).
43. A. Blasco *et al.*, Assessment of neutrophil extracellular traps in coronary thrombus of a case series of patients with COVID-19 and myocardial infarction. *JAMA Cardiol.* **6**, 469–474 (2020).
44. L. Nicolai *et al.*, Immunothrombotic dysregulation in COVID-19 pneumonia is associated with respiratory failure and coagulopathy. *Circulation* **142**, 1176–1189 (2020).
45. V. Chilunda *et al.*, Transcriptional changes in CD16+ monocytes may contribute to the pathogenesis of COVID-19. *Front. Immunol.* **12**, 665773 (2021).
46. M. L. Meizlish *et al.*, A neutrophil activation signature predicts critical illness and mortality in COVID-19. *Blood Adv.* **5**, 1164–1177 (2021).
47. P. Patil *et al.*, Molecular insights on the possible role of annexin A2 in COVID-19 pathogenesis and post-infection complications. *Int. J. Mol. Sci.* **22**, 11028 (2021).
48. A. Aburima *et al.*, Thrombospondin-1 promotes hemostasis through modulation of cAMP signaling in blood platelets. *Blood* **137**, 678–689 (2021).
49. P. Prakash, P. P. Kulkarni, A. K. Chauhan, Thrombospondin 1 requires von Willebrand factor to modulate arterial thrombosis in mice. *Blood* **125**, 399–406 (2015).
50. S. E. Ward *et al.*; Irish COVID-19 Vasculopathy Study (iCVS) investigators, ADAMTS13 regulation of VWF multimer distribution in severe COVID-19. *J. Thromb. Haemost.* **19**, 1914–1921 (2021).
51. T. Hadid, Z. Kafri, A. Al-Katib, Coagulation and anticoagulation in COVID-19. *Blood Rev.* **47**, 100761 (2021).
52. S. S. Adam, N. S. Key, C. S. Greenberg, D-dimer antigen: Current concepts and future prospects. *Blood* **113**, 2878–2887 (2009).
53. L. Hoste *et al.*; MIS-C Clinicians, TIM3+ TRBV11-2 T cells and IFNγ signature in patrolling monocytes and CD16+ NK cells delineate MIS-C. *J. Exp. Med.* **219**, e20211381 (2022).
54. World Health Organization, R&D Blueprint: Novel coronavirus: COVID-19 therapeutic trial synopsis. (2020). https://www.who.int/publications/i/item/covid-19-therapeutic-trial-synopsis (2022/7/5)
55. M. Kiuchi, Elevated Myl9 reflects the Myl9-containing microthrombi in SARS-CoV-2-induced exudative vasculitis and predicts COVID-19 severity. Gene Expression Omnibus. https://www.ncbi.nlm.nih.gov/geo/query/acc.cgi?acc=GSE208337. Deposited 16 July 2022.